Yield strength determination based on dissipative energetic transition

Martin Lesueur[a,*], Xinrui Zhang[a], Hadrien Rattez[b], Tomasz Hueckel[c]

[a] *Civil Engineering and Geosciences, Delft University of Technology, Delft, Netherlands*
[b] *Institute of Mechanics, Materials and Civil Engineering (IMMC), Université Catholique de Louvain, Louvain-la-Neuve, Belgium*
[c] *Civil and Environmental Engineering Department, Duke University, Durham NC, USA*

Abstract

Mechanical yield strength is one of the most crucial mechanical properties to consider to remain operating in safe elastic regimes. Despite its importance, it remains ambiguous to measure as different disciplines acknowledge different definitions. Most common examples include the deviation from linear elasticity or the peak stress. This difference has significant consequences for the modelling of non-linear deformations since the yield point is the foundation of most plasticity models. We seek to find a criterion that is not empirical in comparison to most but based instead on energetic considerations. Indeed, the transition from elastic to plastic regime corresponds to a transition of energy dissipation. The energy potential we introduce for our new definition of the yield is based on equilibrium theory which states that instability happens when the second derivative of potential energy goes to zero. Practically, we measure this point in time where the maximum of the derivative of the mechanical work is found. The method is examined for numerical simulations and experiments on 3D-printed samples. It shows similarities to the traditional offset method in uniaxial compression but is more accurate and differs at high confinements in the compaction cap. It exhibits consistency with the other energetic yield criterion of Gurson. In the future, we aim to make it a new experimental standard for material mechanical testing.

Keywords: yield strength ; mechanical testing ; yield surface

1. Introduction

The determination of the yield strength of a material is an essential exercise of mechanical characterisation since the property critically dictates the regime of stability of a structure. Commonly known as the limit of elasticity, the point of yield strength is most obvious for the simplest case of ideal non-porous linear elastic and ideally plastic materials, like simple metals for instance. Indeed, experimental compression tests of such materials lead to characteristic stress-strain curves displaying a sharp transition between

*Corresponding author
Email address: m.lesueur@tudelft.nl (Martin Lesueur)

the linear elasticity and plasticity, where strain increases at constant stress. For more complex materials, however, including real geomaterials like porous rocks, strong debates remain about the notion of yield point and its quantitative characterisation. This is well illustrated, for instance, by the various definitions of yield from the sixth edition of the McGraw-Hill Dictionary of Scientific and Technical Terms (Parker, 2003):

- ***yield*** *[MECHANICS] That stress in a material at which plastic deformation occurs.*
- ***yield point*** *[MECHANICS] The lowest stress at which strain increases without increase in stress.*
- ***yield strength*** *[MECHANICS] The stress at which a material exhibits a specified deviation from proportionality of stress and strain.*

The first definition, referred to as **initial yield** in this contribution corresponds to the stress when the first region in the material undergoes plasticity. This value is challenging to estimate in practice (Desrues et al., 2017) as it occurs on the stress-strain curve somewhere during the linear phase and does not correspond therefore to any particular transition of deformation regime. However, the advantage of this point is that it corresponds to the limit of elasticity in the strictest term and therefore does not require any implementation of plasticity to determine it. For this reason, it is a point sought after for topology optimisation algorithms that compute the maximum elastic stress sustained (Lu et al., 2014). The second definition, commonly named **limit load**, refers to the state of collapse of the material globally. At this point, most regions of the material are in plasticity. The last definition is the **macroscopic yield**, which points to the visible limit of linear elasticity at the scale of the sample, and is most commonly used in structure design.

Due to the existence of multiple definitions, we understand that the criterion for the yield strength should be selected on the basis of what it represents and with regards to its intended purpose. Indeed, most modellers use the yield as a key point to fit stress-strain curves. The importance of this point is particularly emphasised by Lin et al. (2020) who could not use the yield strength provided by experiments and instead inverted a lower yield surface that allowed them to fit their model. In this contribution, we are looking for a point indicating the onset of plasticity. The purpose is to be able to model the behaviour below the yield as purely elastic and afterwards as plastic. In that sense, the initial yield is not suitable because the material is still in its phase of linear elasticity afterwards. And conversely the limit load is not adequate either because we are way past the onset of plasticity. It is therefore towards the macroscopic yield strength that we focus on.

The macroscopic yield strength is typically evaluated experimentally from stress-strain curves using the classical offset method (Ross, 1999), i.e. the intersection of the curve with a line parallel to its initial linear-elastic part and shifted by an arbitrary strain threshold. For the sake of reproducible measurements worldwide, this threshold was standardised by published experimental procedures that can be found in ASTM or ISO. The most typical value of strain offset is 0.2%. Despite its popularity, one could argue that this method is not satisfactory because of the existence of this arbitrary parameter which qualifies the method as empirical. Indeed, the value set for the strain offset completely determines the yield strength value as illustrated in Fig. C.9 where

0.02% and 0.04% strain offset are considered to determine the yield and result in large differences in the yield determination. As a consequence, the method is also material dependent, as the strain offset varies depending on the material stiffness. Therefore the value of strain offset differs in the published standards depending on which material they are designed for. In the case of Fig. C.9 for example, 0.02% is more adequate than 0.2% which would return unreasonable values of yield stress, way past the visible deviation from linear elasticity. Different methods are sometimes employed to determine the macroscopic yield strength. For a quick assessment of material's strength, the value of the peak stress (Kovari et al., 1983) or ultimate strength is often considered due to its visual simplicity on the stress-strain curve as the maximum of the curve. The gross approximation in this case is that the hardening part of the deformation regime does not accumulate important irreversible deformations, but this assumption can easily become illegitimate. For dilatant materials during triaxial compression experiments, the yield strength can be determined on the curve of axial stress evolving with volumetric strain (Crawford and Wylie, 1987). It corresponds to the dilation point which is when the volumetric strain becomes null and is representative of the development of micro-cracks in the sample. While not widely used in practice, we note other methods such as ones from Henry et al. (2019) or Christensen (2007). The latter suggests to look at the vanishing second derivative of the stress which points to the inflexion point on the stress-strain curve, indicating the yield point. But this approach has no other foundation than the visually apparent transition of deformation regime. This extensive list demonstrates that no consensus exists to determine the macroscopic yield strength and more complementary methods are being developed to compensate for the fact that only empirical criteria exist.

Currently, only one semi-analytical yield criterion derives from a non-empirical approach. Gurson (1977) defines its yield as a potential of maximum plastic dissipation, under the assumption that the full solid domain is assumed to be at yield, from which he can derive a yield criterion using limit analysis. Note that this corresponds to an upper bound of plasticity and refers to the limit load as mentioned previously. Unfortunately, this yield criterion has only been derived for simple structures and materials and furthermore points only to the limit load. For this reason, its application to real materials requires a fitting coefficient, which was introduced in a later study of Tvergaard and Needleman (1984). Another theory describing an energetic transition was employed by Bigoni and Hueckel (1991) who introduced a necessary but non-sufficient indicator for localisation. The point is found when the second-order work vanishes and it has been associated to a burst of kinetic energy by Nicot and Darve (2015). The definition has been extended to unsaturated soils by Buscarnera and di Prisco (2010). This point does not correspond however to the macroscopic yield strength since the onset of localisation happens later, most often after the peak stress in the softening regime.

In this contribution, we search for a similar energetic indicator that would serve as a new definition of the macroscopic yield strength. Indeed, it is particularly attractive to identify the yielding as an energetic transition, since elasticity stores energy, whereas plasticity dissipates energy. We can therefore consider elasticity the storage of potential energy for mechanics. As such from thermodynamics principles, we know that a loss of equilibrium in the system, which would correspond to plasticity, is obtained when the second derivative of the potential energy goes to zero. We investigate in this contribution whether this energetic metric can point to a more representative macroscopic yield strength. Please note as a clarification that we discuss in this contribution about the

definition of the yield point, which is different from the yield criterion, inherent to a material's model, like Mohr-Coulomb, Drücker-Prager or Cam-Clay for example. Ultimately, our method should measure yield surfaces closer to the correct material's model and therefore help characterise those yield criteria more accurately. In a first section, the new method is applied to the simplest porous material that is Gurson's hollow sphere model and we compare our results with other current methods. Then, we test whether the method performs equally well on a real porous material, 3D printed, by determining the yield from experimental compression tests.

2. Comparison to existing methods

2.1. Numerical case study set-up

In this section, we compare the new method introduced in this contribution with existing ones, to distinguish similarities and differences. The case study chosen corresponds to the most idealised porous structure – the hollow sphere geometry – which is constituted of one spherical void. While every definition of yield corresponds unambiguously to the same yield point for non-porous materials, the hollow sphere model introduces enough complexity to separate the different yield points, allowing for a valuable comparison. The structure was also selected by Gurson for the derivation of its yield criterion, which allows to add this yield surface of interest to our comparison.

The hollow sphere consists in a layer of solid matrix delimited by two spheres: the outer one with a radius R_{out} and the inner one with a radius R_{in}. The porosity of the system is $\phi = (\frac{R_{in}}{R_{out}})^3$. The spherical layer is meshed for Finite Elements simulations in spherical coordinates with hexahedra of the second order using the software Gmsh (Geuzaine and Remacle, 2009). The use of spherical coordinates allows to get a good mesh quality as can be seen on Fig. 1 indicated by a signed inverse condition number close to one, the value for a perfectly shaped element.

Yield points can be inferred from the results of mechanical loading simulations in Finite Element on the chosen structure. Different stress paths are imposed to be able to discretely trace the whole yield surfaces. The simulations are carried out with an elasto-plastic Finite Element simulator, introduced in Lesueur et al. (2017), which solves for the momentum balance, reduced to the divergence of stress equals to zero. Since the limit analysis used to derive Gurson's yield criterion is performed on a rigid material, we approach these conditions by choosing a large value of Young's modulus at 200 GPa, along with Poisson ratio of 0.3 and yield stress of 100 MPa. As such, a small strain formulation is sufficient since the mesh deformation remains minimal. In order to retrieve exclusively the effect of porosity on the behaviour of the material, the constitutive model for plasticity is taken as ideal, which implies a $J2$ (or von-Mises) rate-independent plasticity model with no hardening or softening.

As boundary conditions, we impose a constant deformation rate on the outer layer of the sphere. This enforces the Hill-Mandel condition, necessary for a rigorous homogenisation. The velocities imposed on the sphere are inspired from Fritzen et al. (2012) and expressed as

$$v_x = \dot{\varepsilon}_0(\alpha + \beta)x, \tag{1}$$

$$v_y = \dot{\varepsilon}_0(-\alpha + \beta)y, \tag{2}$$

$$v_z = \dot{\varepsilon}_0\beta z \tag{3}$$

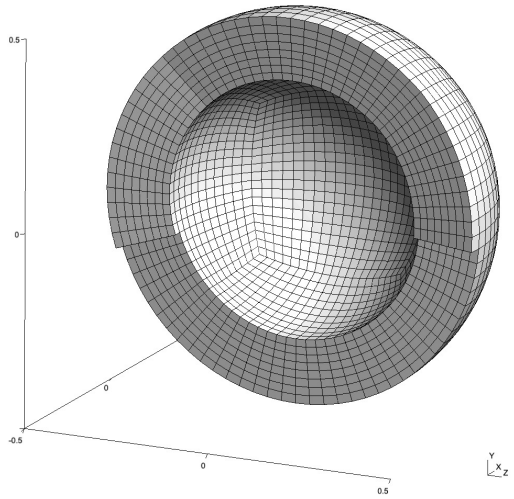

Figure 1: Mesh of the hollow sphere with a porosity of 30%, showing only half for visualisation purposes. It is composed of 8 layers of elements amounting to a total of 19,200 elements. The signed inverse condition number for the mesh is higher or equal than 0.867.

with $\dot{\varepsilon}_0$ the reference loading strain rate and α and β parameters controlling the triaxiality of the stress path, governed by the ratio $\frac{\alpha}{\beta}$.

Having respected the Hill-Mandel condition, the macroscopic values of stress can be defined classically as

$$\sigma_{ij} = \langle \tilde{\sigma}_{ij} \rangle_\Omega = (1-n) \langle \tilde{\sigma}_{ij} \rangle_{\Omega_M} \tag{4}$$

with n the porosity and $\langle \cdot \rangle_\Omega = \frac{1}{|\Omega|} \int_\Omega \cdot dV$, Ω_M being only the matrix material domain. More specifically, we are interested in the mean and Von Mises stress to map the yield surface in the p-q space. They are defined as $p = \sigma_{ii}$ and $q = \sqrt{\frac{3}{2} s_{ij} s_{ij}}$ with s_{ij} being the deviatoric stress tensor.

2.2. Energetic yield method

As per our new definition of macroscopic yield stress, we are looking for the stress value at which the second derivative of the potential energy becomes null. The potential energy in our mechanical system is described as the work induced by the deformations, expressed as $\sigma \cdot \epsilon$. To reduce the approximation made by employing algorithms of numerical differentiation to obtain the vanishing second derivative of the mechanical work, we find equivalently the maximum value of the first derivative of the mechanical work. The evolution of the mechanical work derivative with loading time for the set-up described in the previous subsection is shown in Fig. 2a. In the beginning of the curve, we can observe energy storage as the derivative of the mechanical work increase with a constant slope given by the stiffness of the material. At the limit state the derivative of the mechanical work is constant, indicating that the regime has completely switched to dissipative. For an ideal material, this transition is sharp and happens exactly at the yield like it is shown in the figure of our graphical abstract. For this more complex material, the transition

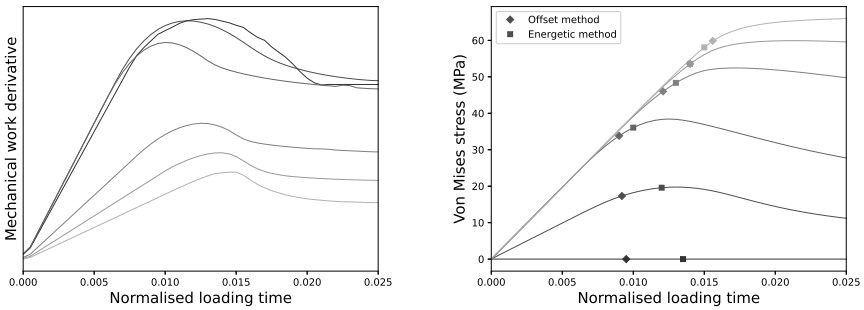

Figure 2: Derivative of the mechanical work for different loading paths (left). The corresponding stress-strain curves are plotted on the right. The yield points determined with both the offset method and our energetic method are marked on the stress-strain curves.

is smooth. It is the point of maximum that best represents this transition and that we define as the macroscopic yield strength. As can be observed, all curves show the same pattern and the maximum can be easily identified. The yield point corresponding to the maximum is reported on the corresponding stress-strain curve in Fig. 2b.

2.3. Results and discussion

The other yields are measured following the methodologies explained in details in Appendix A, Appendix B and Appendix C. Fig. 3 superposes the four envelopes in the $p - q$ space. As mentioned previously, Gurson's upper bound limit load analysis provides the limit state, an upper bound to all possible yield envelope, while the strictest definition provides the initial yield, a corresponding lower bound. We see indeed that all other curves, like the yield surfaces determined by the offset or the energetic method fall indeed in between. It is important to note that the yield surface for the limit state would not be an upper bound if the material displayed a softening regime.

The respective shapes of the four yield envelopes plotted on Fig. 3 provide some interesting information. Simple scaling coefficients are not necessarily enough to transform one yield curve into another. For example, the lower yield exhibits a quasi-linear relationship for stress paths close to isotropic compression, whereas all other curves remain elliptic. Only the upper and energetic envelopes seem to be scaled from one another. This reflects the consistency between the two approaches that are based on energy considerations and this result shows that our method describes a similar energy potential as Gurson's. The yield surfaces do not superpose however because Gurson is looking for maximum energy dissipation which happens at a different timing. We mentioned in the introduction that Gurson's yield criterion seemed to fit quite well the yield surface shape of real materials, but Tvergaard and Needleman (1984) noticed that the order of magnitude of strength predicted was too high which tempted them to introduce a reducing factor q_1 to match real experiments. We show in Appendix D that it is possible to fit the yield surface determined with our method with this extended yield criterion, using a reasonable set of parameters. In that case, we could hypothesise that previous research studies may have mistakenly matched the yield definition we introduce here instead of Gurson's original yield criterion, which is less commonly measured.

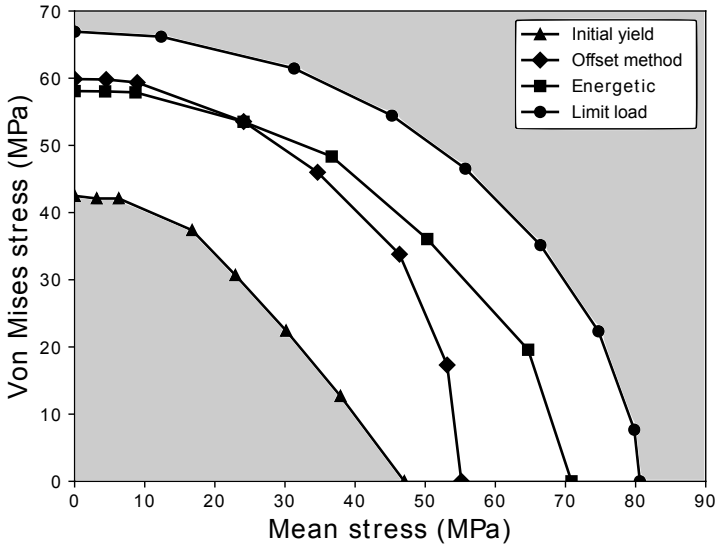

Figure 3: Different yield surfaces considered in this contribution plotted in the $p-q$ space for the hollow sphere of porosity ϕ=30%.

The important comparison in this contribution is between the offset method which is commonly used and the new method we introduce, which is based on a more scientifically sound energetic criterion. In the dilatant shear regime, the two methods return very similar yield stress values. This means that for uniaxial compression tests, which are the most common mechanical tests performed, the offset method gives reasonably energetically accurate values. However, we observe a difference later in the compactive regime where the offset method underestimates the yield stress. The empirical concept of deviation from linear elasticity does not seem to match the energetical transition which happens considerably later as can be observed in the lower curves of Fig. 2b.

3. Experimental validation

3.1. Experimental case study set-up

The previous section presented our new method to determine the macroscopic yield stress and showed the advantages it presents in comparison to the classical method. The first step of validation was done for a virtual material, rigid and ideally plastic. We aim now to further validate the method against a real material because of its added complexity. We choose 3D printed polylactic acid (PLA) which presents a non-trivial rheology, notably viscoplasticity and can display both hardening and softening during mechanical loading. 3D printing allows for a complete control of the structure of the manufactured part. We choose to continue using Gurson's hollow sphere model in this section which adds the complexity of the structure on top of the one of the rheology and is illustrated by the presence of the compaction cap in the yield surface. To facilitate the

printing process, we simplify the structure to 2D which reduces the hollow sphere with a spherical void to a hollow cylinder with a cylindrical void, and can easily be 3D printed in the vertical direction.

The samples are printed by Fused Deposition Modelling (FDM) on the Ultimaker 2+, the most common customer-level 3D-printer. Layer thickness and line width of each filament are set as 0.4 mm and 0.6 mm respectively. The printing speed when the nozzle is extruding material within the printed part is 40 mm/s, while this speed is 30 mm/s when the nozzle is extruding to fabricate the outer wall encircling the printed part. The travelling speed when the nozzle is moving without extruding material is 200 mm/s with a 205^o printing temperature to smoothen the surface of the printed part. The solid regions, non-porous, are printed with 100% infill density. Despite setting that printing parameter, the FDM process is known to generate micro-porosity, because of which the mechanical properties of the part deviate from the PLA filament manufacturer indication. This requires us to establish a calibration of the 3D printed PLA mechanical properties. Following this step further detailed in Lesueur et al. (2021), an ideal elasto-plastic model of the 3D printed PLA is obtained with a Young's modulus of 1700 MPa and a macroscopic yield strength of 46.3 MPa. Note that this calibration process is only needed to compare the measured yield to the corresponding simulation and Gurson's criterion, which require both the knowledge of the solid material constitutive model.

To characterise the whole yield surface, the samples are tested on a triaxial compression machine from the Multiphysics Geomechanics Laboratory in Duke University at different confinements (0, 10, 20, 30 and 35 MPa) at a constant loading rate of 0.096 mm/min to dismiss the rate dependency of the viscous plastic. In the previous numerical section, the true values of the macroscopic stress tensor could be rigorously homogenised. Experimentally, the set-up only allows to retrieve the force experienced by the sample on the top boundary F_{top} and the confining pressure P_{conf}. However, given our axisymmetric structure, the stress experienced by the top surface is representative of the whole volume. The Von Mises stress in a triaxial set-up simplifies to

$$\sigma_1 - \sigma_3 = (\frac{F_{top}}{\pi R^2} + P_{conf}) - P_{conf} = \frac{F_{top}}{\pi R^2}. \tag{5}$$

An example of the stress-strain curve obtained is displayed in Fig. 4.

3.2. Experimental determination of yield

Sec. 2.2 had defined a new indicator to get the value of the macroscopic yield. In this section, we verify that the theory also applies for real experiments and here suggest a new experimental protocol to measure the macroscopic yield.

Sec. 2.2 showed that we could define the macroscopic yield as an energetic transition as the stress corresponding to the vanishing second derivative of the mechanical work. In order to keep the number of derivatives to a minimum, we are looking instead equivalently for the maximum of the first derivative. The mechanical work is expressed as $\varepsilon_{11}\sigma_{11} + \varepsilon_{22}\sigma_{22} + \varepsilon_{33}\sigma_{33}$. In the case of triaxial compression, the confining pressure is constant and the radial strain is negligible compared to the axial variation. The derivative of the mechanical work with loading time or strain reduces to the derivative of the axial component $\varepsilon_{11}\sigma_{11}$. It is important to note that the method does not require therefore any new measurements to be applied than for traditional mechanical testing.

The derivative of the mechanical work can be roughly but directly obtained on the raw data by doing a discrete differentiation of the data. This is adequate for the numerical data of the previous section which is nicely smooth. However, experimental datasets always incorporate some level of noise, which renders the straightforward derivative unsuitable since the maximum cannot be interpreted from the noisy signal, as shown in Fig. 4. Instead, we advise to apply numerical processing to obtain a smoother curve. As a suggestion, we turn to machine learning to fit the curve of the mechanical work using a gaussian process, which is known to be indefinitely differentiable. We use premade functions from the Python module GPytorch, implemented in Pytorch (Paszke et al., 2019). The interpolation is done in dimensionless space and we iterate until convergence of the loss, length-scale and noise. The advantage of this method is the flexibility to adapt to any data series and therefore can accommodate any level of noise. Being infinitely differentiable, the derivative obtained is smooth and the maximum is unambiguous as can be observed in Fig. 4.

3.3. Results and discussion

Using the method of the previous subsection, the values of the macroscopic yield are found for each experiment of different confining pressure and are reported in Fig. 5, delineating the shape of the yield surface.

Since the structure considered corresponds to the geometry modelled by Gurson, we can plot in comparison the limit load yield surface of Gurson. It is modelled with the porosity considered in this study, 0.25 and the yield strength of the 3D printed material, calibrated in Sec. 3.1. While the first point at zero confinement, corresponding to the uniaxial compression, matches the analytical solution, all of the others deviate from the trend. The difference with uniaxial compression, in which only the axial load varies is that when confinement is applied, the stress in the radial direction also increases. Gurson formulated his model considering an isotropic material. Instead, the FDM process generates an anisotropic material, more specifically orthotropic where the printing direction is weaker than the lateral ones because of the layering printing process. Liao et al. (1997) were interested to take into account this anisotropic behaviour and extended Gurson's model to anisotropic materials. We manage to fit this model to our experimental dataset with a orthotropic ratio of 0.75. As seen in Fig. 5, the experimental points now fit exactly this analytical yield surface.

Following the method from Lesueur et al. (2021), we can also predict the macroscopic yield stress from simulation, knowing the structure (hollow cylinder) and the material parameters, obtained from a calibration on a full sample, detailed in the beginning of this section. This anisotropy was not taken into account in Lesueur et al. (2021) because it does not affect uniaxial compression as mentioned previously. The orthotropy of the yield strength is modelled following Yoon et al. (2014), implemented in MOOSE (Permann et al., 2020). The anisotropic ratio was taken to be 0.75 and the perfect match between the experimental and numerical results confirms once again that the ratio is correct.

From the stress-strain curves, we can apply the offset method as done commonly to measure the macroscopic yield. To obtain reasonable values, we apply a strain offset of 0.1% because 0.2% returns points too far in the plasticity regime. The yield points that are obtained fall at the same spot than the ones our energetic method returns. Compared to Fig. 3, the two methods do not diverge yet in the more compactive regime. This could be explained by the fact that the stress strain curves still display a sharp transition

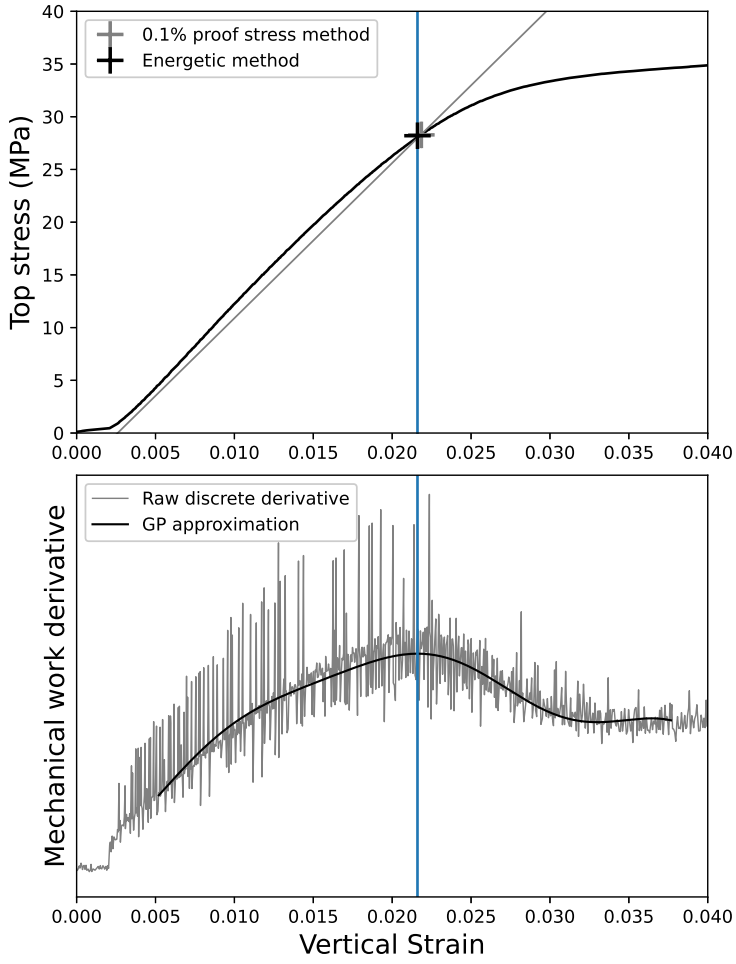

Figure 4: Experimental protocol to measure the yield as the maximum point of the mechanical work derivative. Traditional experimental protocol is plotted in comparison.

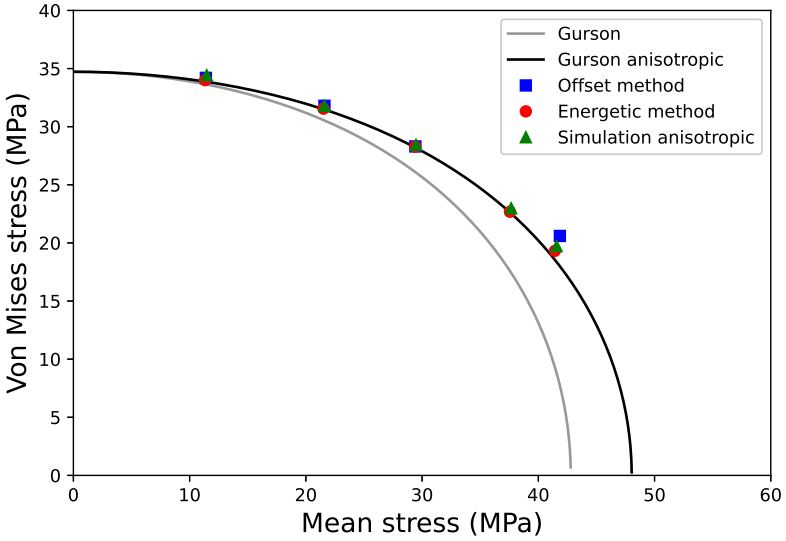

Figure 5: Yield surfaces obtained from experiments on 3D-printed samples, compared with Gurson's yield criterion and results from numerical simulations.

from elasticity to plasticity even at the highest confining pressure. Considering the curves of Fig. 2b, we can expect that the two methods would differ when the hardening of the stress-strain curve becomes softer in the compactive regime. We notice that the last point on the yield surface slightly deviates from the obtained results so far. As we reach the compaction cap with increasing confining pressure, the yield strength decreases. And the range of elasticity for which the Young's modulus can be measured is reduced correspondingly. Since the consolidation part of the curve at early strains also remains present, it becomes harder and harder to measure the elastic slope, which in turn reduces the results accuracy of the offset method. This can be seen in Fig. 4 where the determination of the elastic slope can be ambiguous. When measured too early, one might find a deviation due to the initial consolidation. When measured too late, one might find a deviation due to the plasticity developing. In contrast, our method does not require the determination of the Young's modulus and is therefore not prone to this issue.

This final section showed that the new method can easily be used to determine the macroscopic yield stress of experimental stress-strain curves. We note that more processing to smooth the inherent noise of experimental data-series may be needed to find the maximum of the derivative of the mechanical work. Eventually, the perfect match with the simulation confirms the validity of the method experimentally. As an extra validation, we confirm again that the energy potential matches Gurson's.

4. Conclusion

In this contribution we introduced a method to determine the macroscopic yield strength, corresponding to the onset of plasticity. The new indicator is based on thermodynamics loss of equilibrium and corresponds to the maximum of the derivative of the mechanical work, describing the energetic transition from elasticity to plasticity. Compared to the previous methods used which are all empirical, this method is more scientifically rigorous and the energy potential it describes is similar to the semi-analytical criterion introduced by Gurson (1977), which showed great applicability on real materials.

For its application, the method does not require any different measurements than traditional mechanical tests but some postprocessing is needed for the differentiation of the data series. Compared to the traditional offset method, it does not require the knowledge of the material's stiffness which makes it more accurate. In this study, the limits of the offset method are highlighted in the late compaction regime, where the yield stress is found consistently lower than with our method. In regards to the recent work of the authors, this method will prove extremely useful to improve the accuracy of the yield surfaces determined numerically on digital rocks (Lesueur et al., 2022). With the help of more numerous and diverse experimental validations, we can aspire to make this method an experimental standard for macroscopic yield strength determination.

Acknowledgements

We thank Dr. Iuri Rocha for helping us develop the script of gaussian process approximation.

Appendix A. Limit load - Gurson's benchmark

We defined the limit load as the *"lowest stress at which strain increases without increase in stress"*. Mechanical simulations are run until the stress-strain curve has reached its ultimate state, i.e. stresses have converged to the limit load values. We perform the triaxial extension simulation for various combinations of α and β. Fig. A.6 shows that for every simulation, both the macroscopic mean stress and Von Mises stress converge before the normalised time reaches one.

The limit load values of $\overline{p}$ and $\overline{q}$ (at $t = 1$) from all simulations are then plotted on Fig. A.7 as separate points in the $p - q$ space to form the yield surface obtained numerically for this hollow sphere. The results are then compared with Gurson's yield criterion, derived through limit analysis and expressed as

$$\frac{\overline{q}^2}{\overline{\sigma}_0^2} + 2\phi cosh(\frac{3}{2}\frac{\overline{p}}{\overline{\sigma}_0}) - 1 - \phi^2 = 0 \tag{A.1}$$

The whole exercise is repeated for a different value of porosity of 12.5% and the results are also plotted on Fig. A.7.

For both scenarios ($\phi = 30\%$ and $\phi = 12.5\%$), Fig. A.7 shows reasonable matches between our numerical results and Gurson's upper bound approximation, with Gurson's curve naturally falling above the yield envelope computed numerically. The difference

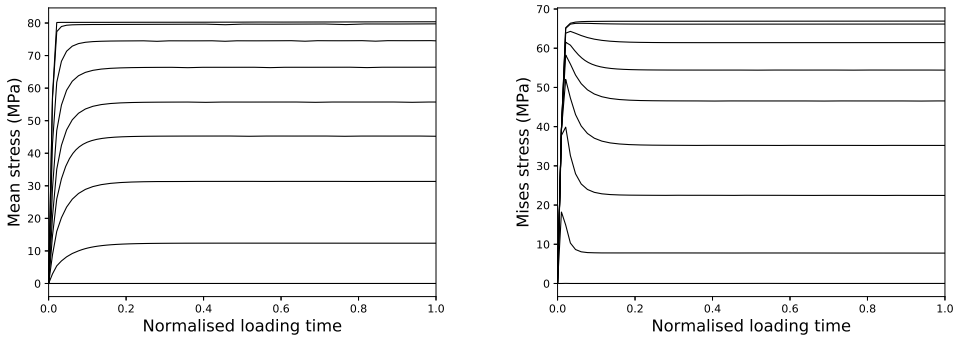

Figure A.6: Mean (left) and Von Mises (right) Stress vs loading time for the hollow sphere of Fig. 1, following various loading paths obtained for different combinations of (α, β). The graph on the left-hand side goes from pure shear to isotropic compression from the bottom to the top and the other way around for the graph on the right hand side.

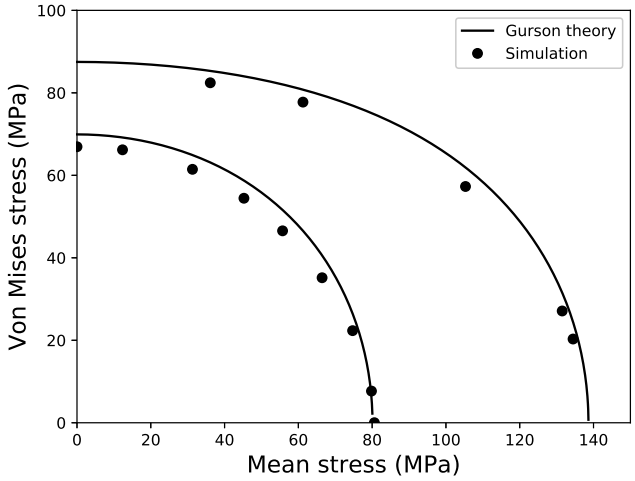

Figure A.7: Yield surface of the hollow sphere in the $p-q$ space for two different porosities ϕ=30% and 12.5%. The results of our simulation are compared with Gurson's yield criterion.

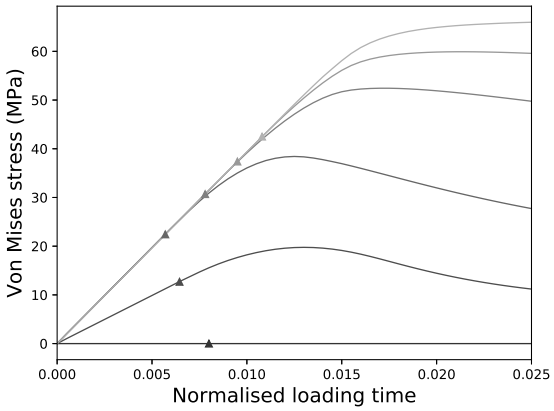

Figure B.8: Lower yield surface for the hollow sphere of porosity ϕ=30% obtained under the loading boundary conditions of Eq. 3 for various triaxial ratios.

between both curves even allows us to quantify the (relatively constrained) approximation error coming from Gurson's upper bound approximation of the dissipation, since the full numerical simulations computed the exact yield surface within a very strict numerical tolerance.

Appendix B. Initial yield

We study the strictest yield, by selecting a different definition, *"that stress in a material at which plastic deformation occurs"*. This definition focuses on the exact onset of plasticity, a concept more relevant from a mathematical point of view than an experimental perspective. Contrarily to the experimental viewpoint, the occurrence of the first irreversible deformation in the material is easy to compute numerically, with the timing of the event determined by the first element of the mesh that enters plasticity. In our hollow sphere model, since the pore acts as a weakness for the material, the stress concentrates around the pore and the first element to enter the plastic regime will therefore be located on the inner spherical surface of the model for any of the admissible loading paths considered. For this reason, the mesh used to determine this lower yield is modified from the one shown in Fig. 1, keeping the same number of elements but with a different radial distribution of element thicknesses, with finer elements towards the centre of the sphere to capture the onset of plasticity more precisely.

The results are plotted on Fig. 3, which shows that this yield surface has a different shape from Gurson's. While the behaviour is similar for shearing stress paths, the lower yield surface becomes almost linear in $p - q$ for loadings that are more isotropic.

Appendix C. Offset method

Appendix A and Appendix B are particularly useful as they provide bounds of the admissible range of yield envelopes that could be obtained with any existing or new

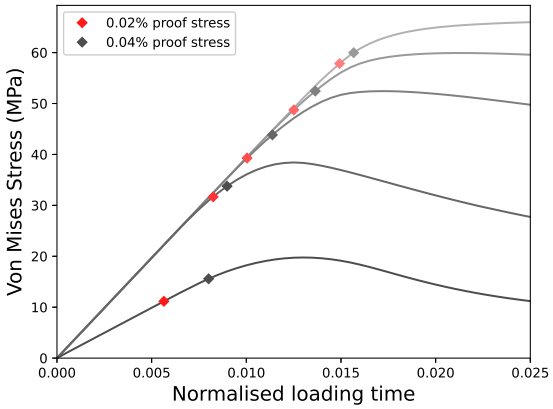

Figure C.9: Yield points measured with the offset method considering two values of proof stress, for the hollow sphere of porosity ϕ=30% obtained under the loading boundary conditions of Eq. 3 for various triaxial ratios.

definition. For practical purposes, however, experimentalists rely instead on the third definition of the yield stated in the introduction, *"the stress at which a material exhibits a specified deviation from proportionality of stress and strain"*.

This definition, which assumes that the material behaves linearly in elasticity, is more subjective than the previous two since the *deviation from proportionality* cannot be determined in a unique manner on real measurement data. This *experimental* yield is usually identified graphically on the stress-strain curve and it requires the specification of an ad-hoc strain threshold X, given by ASTM standards and typically of 0.1, 0.2 or 0.5% (ASTM E8/E8M-16a, 2016). An offset method, often called *X % proof stress* (Ross, 1999), then determines the yield as the intersection of the stress-strain curve with a line parallel to the initial linear-elastic part of that stress-strain curve, shifted by the amount of strain X (see Fig. 4).

Since our virtual material is taken as extremely rigid and does not correspond to any ASTM standard, we will consider an arbitrarily small offset of 0.04% of plastic strain of deviation. The identified experimental yields for several loading paths on the hollow sphere are reported on Fig. C.9.

Appendix D. Gurson-Tvergaard-Needleman

The Gurson-Tvergaard-Needleman (GTN) model (Tvergaard, 1981), introduced as an extension of the Gurson's yield criterion, has proven to match real observations with better fidelity. The model is expressed as

$$\frac{\overline{q}^2}{\overline{\sigma}_0^2} + 2\phi q_1 cosh(\frac{3q_2}{2}\frac{\overline{p}}{\overline{\sigma}_0}) - 1 - q_3\phi^2 = 0, \tag{D.1}$$

introducing three flexible parameters q_1, q_2, q_3. Techniques were developed to be able to fit those material parameters (Springmann and Kuna, 2005; Oral et al., 2010; Zhang

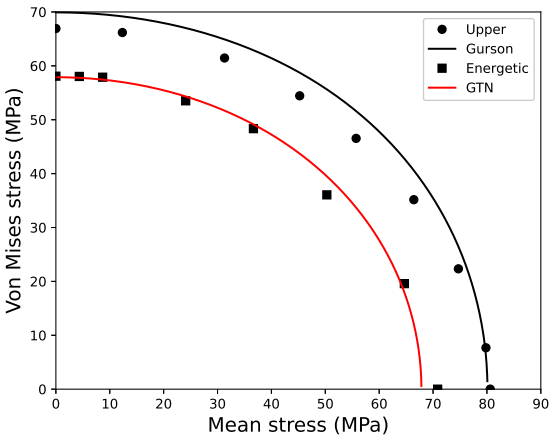

Figure D.10: Fit of the energetic yield surface with the GTN model, for the hollow sphere system described in Sec.2.1.

et al., 2021). In Fig. D.10, we show that we obtain a good fit with the GTN model using $q_1 = 1.4$, $q_2 = 0.85$ and $q_3 = 1.96$. Those parameters values remain in the range expected from the literature. Most commonly, $q_3 = q_1^2$ (Tvergaard, 1981), $q_1 = 1.25 - 2$ and $q_2 \approx 1$ (Besson et al., 2004).

References

ASTM E8/E8M-16a, 2016. Standard Test Methods for Tension Testing of Metallic Materials. Technical Report. ASTM International. doi:10.1520/e0008_e0008m-16a.

Besson, J., Berdin, C., Bugat, S., Feyel, F., Forest, S., Pineau, A., 2004. Local approach to fracture. Science de la matière, Presse des Mines.

Bigoni, D., Hueckel, T., 1991. Uniqueness and localization—i. associative and non-associative elastoplasticity. International Journal of Solids and Structures 28, 197–213. doi:10.1016/0020-7683(91)90205-t.

Buscarnera, G., di Prisco, C., 2010. Discussing the definition of the second-order work for unsaturated soils. International Journal for Numerical and Analytical Methods in Geomechanics 36, 36–49. doi:10.1002/nag.991.

Christensen, R.M., 2007. Observations on the definition of yield stress. Acta Mech. 196, 239–244. doi:https://dx.doi.org/10.1007/s00707-007-0478-0.

Crawford, A., Wylie, D., 1987. Modified multiple failure state triaxial testing method, in: 28th US Symposium on Rock Mechanics.

Desrues, J., Andò, E., Bésuelle, P., Viggiani, G., Debove, L., Charrier, P., Toni, J.B., 2017. Localisation precursors in geomaterials?, in: Springer Series in Geomechanics and Geoengineering. Springer International Publishing, pp. 3–10. doi:https://dx.doi.org/10.1007/978-3-319-56397-8_1.

Fritzen, F., Forest, S., Böhlke, T., Kondo, D., Kanit, T., 2012. Computational homogenization of elastoplastic porous metals. Int. J. Plast. 29, 102–119. doi:https://dx.doi.org/10.1016/j.ijplas.2011.08.005.

Geuzaine, C., Remacle, J.F., 2009. Gmsh: A 3-d finite element mesh generator with built-in pre- and post-processing facilities. International Journal for Numerical Methods in Engineering 79, 1309–1331. doi:10.1002/nme.2579.

Gurson, A.L., 1977. Continuum theory of ductile rupture by void nucleation and growth: Part i—yield criteria and flow rules for porous ductile media. J. Eng. Mater. Technol. 99, 2–15. doi:https://dx.doi.org/10.1115/1.3443401.

Henry, C., Rupel, K., Park, C., Costanzo, J., Kaczowka, C., Malik, K., Ghose, S., 2019. Evaluation of an alternate method for determining yield strength offset values for selective laser sintered polymeric materials, in: SAMPE 2019 - Charlotte, NC, SAMPE. doi:10.33599/nasampe/s.19.1583.

Kovari, K., Tisa, A., Einstein, H., Franklin, J., 1983. Suggested methods for determining the strength of rock materials in triaxial compression: Revised version. International Journal of Rock Mechanics and Mining Sciences & Geomechanics Abstracts 20, 285–290. doi:10.1016/0148-9062(83)90598-3.

Lesueur, M., Casadiego, M.C., Veveakis, M., Poulet, T., 2017. Modelling fluid-microstructure interaction on elasto-visco-plastic digital rocks. Geomechanics for Energy and the Environment 12, 1–13. doi:https://dx.doi.org/10.1016/j.gete.2017.08.001.

Lesueur, M., Poulet, T., Veveakis, M., 2021. Predicting the yield strength of a 3d printed porous material from its internal geometry. Additive Manufacturing 44, 102061. doi:10.1016/j.addma.2021.102061.

Lesueur, M., Veveakis, M., Rattez, H., 2022. Influence of cementation on the yield surface of rocks numerically determined from digital microstructures. International Journal of Plasticity 156, 103338. doi:10.1016/j.ijplas.2022.103338.

Liao, K.C., Pan, J., Tang, S., 1997. Approximate yield criteria for anisotropic porous ductile sheet metals. Mechanics of Materials 26, 213–226. doi:10.1016/s0167-6636(97)00033-1.

Lin, J., Sari, M., Alevizos, S., Veveakis, M., Poulet, T., 2020. A heuristic model inversion for coupled thermo-hydro-mechanical modelling of triaxial experiments. Computers and Geotechnics 117, 103278. doi:https://dx.doi.org/10.1016/j.compgeo.2019.103278.

Lu, L., Sharf, A., Zhao, H., Wei, Y., Fan, Q., Chen, X., Savoye, Y., Tu, C., Cohen-Or, D., Chen, B., 2014. Build-to-last: Strength to weight 3d printed objects. ACM Transactions on Graphics 33, 1–10. doi:10.1145/2601097.2601168.

Nicot, F., Darve, F., 2015. Describing failure in geomaterials using second-order work approach. Water Science and Engineering 8, 89–95. doi:10.1016/j.wse.2015.05.001.

Oral, A., Anlas, G., Lambros, J., 2010. Determination of gurson–tvergaard–needleman model parameters for failure of a polymeric material. International Journal of Damage Mechanics 21, 3–25. doi:10.1177/1056789510385261.

Parker, S.P., 2003. McGraw-Hill Dictionary of Scientific and Technical Terms. Sixth ed., New York : McGraw-Hill.

Paszke, A., Gross, S., Massa, F., Lerer, A., Bradbury, J., Chanan, G., Killeen, T., Lin, Z., Gimelshein, N., Antiga, L., Desmaison, A., Köpf, A., Yang, E., DeVito, Z., Raison, M., Tejani, A., Chilamkurthy, S., Steiner, B., Fang, L., Bai, J., Chintala, S., 2019. Pytorch: An imperative style, high-performance deep learning library. doi:10.48550/ARXIV.1912.01703.

Permann, C.J., Gaston, D.R., Andrš, D., Carlsen, R.W., Kong, F., Lindsay, A.D., Miller, J.M., Peterson, J.W., Slaughter, A.E., Stogner, R.H., Martineau, R.C., 2020. MOOSE: Enabling massively parallel multiphysics simulation. SoftwareX 11, 100430. URL: http://www.sciencedirect.com/science/article/pii/S2352711019302973, doi:https://doi.org/10.1016/j.softx.2020.100430.

Ross, C.T.F., 1999. Mechanics of Solids. Woodhead Publishing.

Springmann, M., Kuna, M., 2005. Identification of material parameters of the gurson–tvergaard–needleman model by combined experimental and numerical techniques. Computational Materials Science 33, 501–509. doi:https://dx.doi.org/10.1016/j.commatsci.2005.02.002.

Tvergaard, V., 1981. Influence of voids on shear band instabilities under plane strain conditions. Int. J. Fract. 17, 389–407. doi:https://dx.doi.org/10.1007/bf00036191.

Tvergaard, V., Needleman, A., 1984. Analysis of the cup-cone fracture in a round tensile bar. Acta Metallurgica 32, 157–169. doi:10.1016/0001-6160(84)90213-x.

Yoon, J.W., Lou, Y., Yoon, J., Glazoff, M.V., 2014. Asymmetric yield function based on the stress invariants for pressure sensitive metals. International Journal of Plasticity 56, 184–202. doi:10.1016/j.ijplas.2013.11.008.

Zhang, T., Lu, K., Mano, A., Yamaguchi, Y., Katsuyama, J., Li, Y., 2021. A novel method to uniquely determine the parameters in gurson–tvergaard–needleman model. Fatigue & Fracture of Engineering Materials & StructuresLocal approach to fracture 44, 3399–3415. doi:10.1111/ffe.13568.